Journal of Applied Polymer Science

Facile Preparation of Superhydrophobic Polyester Surfaces with Fluoropolymer/SiO_2 Nanocomposites Based on Vinyl Nanosilica Hydrosols

Lihui Xu,[1] Zaisheng Cai,[2] Yong Shen,[1] Liming Wang,[1] Ying Ding[1]
[1]College of Fashion, Shanghai University of Engineering Science, Shanghai 201620, China
[2]College of Chemistry, Chemical Engineering and Biotechnology, Donghua University, Shanghai 201620, China
Correspondence to: L. Xu (E-mail: xulh0915@163.com)

ABSTRACT: A facile method to prepare superhydrophobic fluoropolymer/SiO_2 nanocomposites coating on polyester (PET) fabrics was presented. The vinyl nanosilica (V—SiO_2) hydrosols were prepared via one-step water-based sol-gel reaction with vinyl trimethoxy silane as the precursors in the presence of the base catalyst and composite surfactant. Based on the V—SiO_2 hydrosol, a fluorinated acrylic polymer/silica (FAP/SiO_2) nanocomposite was prepared by emulsion polymerization. The FAP/SiO_2 nanocomposites were coated onto the polyester fabrics by one-step process to achieve superhydrophobic surfaces. The results showed that silica nanoparticles were successfully incorporated into the FAP/SiO_2 nanocomposites, and a specific surface topography and a low surface free energy were simultaneously introduced onto PET fibers. The prepared PET fabric showed excellent superhydrophobicity with a water contact angle of 151.5° for a 5 μL water droplet and a water shedding angle of 12° for a 15 μL. © 2014 Wiley Periodicals, Inc. J. Appl. Polym. Sci. **2014**, *131*, 40340.

KEYWORDS: coatings; composites; polyesters

Received 31 October 2013; accepted 22 December 2013
DOI: 10.1002/app.40340

INTRODUCTION

It is well-known that lotus leaves could make water droplets easily roll off and remove dirt particles in their path. Inspired by lotus leaves, superhydrophobic surfaces with a water contact angle (WCA) bigger than 150° have received tremendous attention recently in both fundamental research and practical applications due to their unique characteristics like self-cleaning, anti-icing, anticontamination, and antisticking. Numerous studies have confirmed that the superhydrophobic surfaces could be achieved by a combination of the surface microstructures/nanostructures and low surface energy materials.[1–3]

Fluorochemicals with their low surface energy are widely used for preparation of hydrophobic surfaces, such as water repellent fabric surfaces. However, it was reported that trifluoromethyl group (CF_3)-terminated flat surfaces with the lowest surface energy exhibited the highest WCA of 110–120°,[4–6] which was much lower than 150°. Therefore, superhydrophobic surfaces could not be achieved only by fluorochemicals treatment.

The surface microstructures/nanostructures can be obtained by introducing inorganic nanosize particles such as SiO_2,[7–11] TiO_2,[12–14] ZnO,[15–17] gold particles,[18] silver particles,[19] alumina particles,[20] and carbon nanotubes.[21,22] Recently, the hybrid materials had been extensively applied to fabricate superhydrophobic surfaces by the cooperation of low surface energy caused by organic materials and rough surface structures due to inorganic nanomaterials.[10,13,23–26] Low cost nanosilica with high strength, high toughness, high temperature resistant, and corrosion resistant could be widely used as inorganic materials to prepare hybrid materials.

Some researchers obtained superhydrophobic surfaces by physically mixing inorganic SiO_2 nanoparticles and polymers.[10,27] However, the main problem is the poor compatibility between inorganic nano SiO_2 materials and organic materials due to SiO_2 nanoparticle aggregation. By embedding hydrophobically modified fumed silica (HMFS) particles in polyvinylidene fluoride (PVDF) matrix, Basu and Paranthaman[28] prepared superhydrophobic PVDF-HMFS hybrid composite coatings. Hsieh et al.[29] fabricated water and oil repellency nanocoatings by well mixing silica nanospheres and perfluoroalkyl methacrylic copolymers. Lakshmi et al.[10] obtained superhydrophobic sol–gel nanocomposite coatings by incorporation of a perfluoroalkylmethacrylic copolymer in a hybrid sol–gel matrix containing fumed silica nanoparticles.

In contrast, some researches prepared superhydrophobic surfaces based on polymers/inorganic nanoparticles composites by using chemical methods.[30,31] Sun et al.[24] prepared excellent superhydrophobic films based on the polystyrene/silica nanoparticles by radical polymerization of silica nanoparticles possessing vinyl groups and styrene with benzoyl peroxide. Qu et al.[32] obtained a superhydrophobic hybrid surface originated from quincunx-shaped composite silica particles. The dual size particles were obtained by using the graft of different modified silica particles with epoxy functional groups and amine functional groups. Cui et al.[33] successfully synthesized SiO_2-fluorinated polyacrylate nanocomposite latex particles by seeded emulsion polymerization of fluorinated monomer and acrylate with vinyltriethoxysilicone (VTES) modified nano-SiO_2 as seeds. Therefore, in order to prepare the polymers/SiO_2 nanocomposites by chemical methods, it is necessary that SiO_2 nanoparticles are modified by introducing active groups such as vinyl, thiol, and amine groups. As a result, with regard to the polymers/SiO_2 nanocomposites the polymer matrix could be chemically bonded with nano SiO_2 by the active groups, leading to the improvement of compatibility between inorganic SiO_2 nanoparticles and polymers.

Nowadays, silane coupling agents are usually used to modify the silica nanoparticles. Two different methods including postgrafting[34–36] and cocondensation[37–39] can be employed. For postgrafting method, pure silica particles are firstly synthesized generally using the classical Stöber method. And then silane coupling agents are covalently crosslinked with nano SiO_2, achieving surface modification by two steps. But the method is complicated with partial surface coverage of functional groups, usually involving excess silane coupling agents. In comparison, the cocondensation method refers to cocondensation of tetraalkoxysilane and organosilane precursors usually using the Stöber method via one-step process. In general, the modified silica particles prepared by the cocondensation method have a higher surface coverage of functional groups. Unfortunately, the Stöber method needs a large amount of organic solvent as the reaction medium, such as alcohol. The organic solvent, which is expensive and inflammable, may cause pollution for the environment.

Compared with the traditional preparation of modified silica particles, in order to simplify the preparation process and avoid the use of organic solvent, vinyl silica (V—SiO_2) hydrosols were prepared in this study by one-step water-based sol-gel method with the composite surfactant emulsification, using vinyl trimethoxy silane (VTMS) as the precursor and ammonium hydroxide as the catalyst. A fluorinated acrylic polymer/nanosilica (FAP/SiO_2) nanocomposite containing short fluoroalkyl chains was prepared via emulsion polymerization based on V—SiO_2 hydrosol. The nano-SiO_2 and FAP were chemically bonded by the vinyl bridge. And then the FAP/SiO_2 nanocomposite was coated onto the polyester (PET) fabric to realize superhydrophobicity. This facile approach is expected to broaden the potential applications of superhydrophobic surfaces.

EXPERIMENTAL

Materials

The twill woven PET fabrics (450 ends/240 picks) were used as substrates with 34 tex warp yarns and 38 tex filling yarns. The weight per unit area of the PET fabric was 195 g/m^2. Sodium dodecyl benzenesulfonate (SDBS), ammonium hydroxide ($NH_3 \cdot H_2O$, 28 wt %), sodium hydrate, ammonium persulfate (APS), butyl acrylate (BA), methyl methacrylate (MMA), and 2-hydroxyethyl acrylate (HEA) were analytical reagents and were purchased from Sinopharm Chemical Reagent (Shanghai, China). Fatty alcohol polyoxyethylene ether (AEO-9) was purchased from Zibo Haijie Chemical (Zibo, Shandong, China). VTMS was obtained from Hangzhou Feidian Chemical (Hangzhou, Zhejiang, China), and dodecafluoroheptyl methacrylate (DFMA) was supplied by Harbin Xeogia Fluorine-Silicon Chemical (Harbin, Heilongjiang, China).

One-Step Preparation of V—SiO_2 Hydrosol

First, VTMS (2 g) and AEO-9/SDBS composite surfactant (AEO-9/SDBS =2/1 wt) were added to 100 mL of water and the mixture was stirred vigorously at 30°C for 90 min to homogenize. The concentration of AEO-9/SDBS composite surfactant was 1.0 CMC (critical micelle concentration). Then 2 mL $NH_3 \cdot H_2O$ was added dropwise and the reaction occurred at 30°C with constant stirring for 4 h to form the V—SiO_2 hydrosol.

Preparation of FAP/SiO_2 Nanocomposites

The FAP/SiO_2 nanocomposite was prepared by emulsion polymerization of acrylate monomers and fluoroacrylic monomer in the presence of V—SiO_2 particles as shown in Figure 1. First, acrylate monomers like BA, MMA, (BA/MMA = 3 : 2 wt) and HEA (2 wt % based on total monomers; the percentages stated below are on the same basis) were mixed with the AEO-9 and SDBS (AEO-9/SDBS = 2/1 wt) as composite emulsifier (4 wt %) and the mixture was stirred vigorously at 50°C for 50 min to obtain the pre-emulsified acrylate monomers mixture. Similarly, the pre-emulsified fluoroacrylic monomer DFMA (20 wt %) was obtained with the above method.

The above prepared V—SiO_2 (6 wt %) and some of the pre-emulsified acrylate monomers mixture were introduced in a four-neck round-bottom flask equipped with a heat exchange system. The mixture was stirred for 30 min. After deairing with nitrogen, when the temperature rose to 60°C, some of the initiator APS (0.8 wt %) was added drop by drop slowly into the reactants. After 30 min, the reaction temperature rose to 80°C. And then the residual pre-emulsified acrylate monomers mixture and the pre-emulsified DFMA monomer were slowly and successively dropped into the reaction system. Simultaneously, the residual initiator APS was added dropwise. Afterwards, the polymerization was carried out at 80°C for another 4 h. Then the FAP/SiO_2 nanocomposites were obtained.

In addition, the FAP containing short fluoroalkyl chains without V—SiO_2 particles was also prepared by conventional emulsion copolymerization using the same amount of acrylate monomers, fluoroacrylic monomer, initiator APS, and AEO-9/SDBS composite emulsifier.

Treatment of PET Fabrics

The FAP/SiO_2 nanocomposites were coated onto the PET fabric samples by dip-pad-cure process. The PET fabrics were immersed in the obtained FAP/SiO_2 nanocomposites and FAP at the same concentration of 60 g/L at ambient temperature for

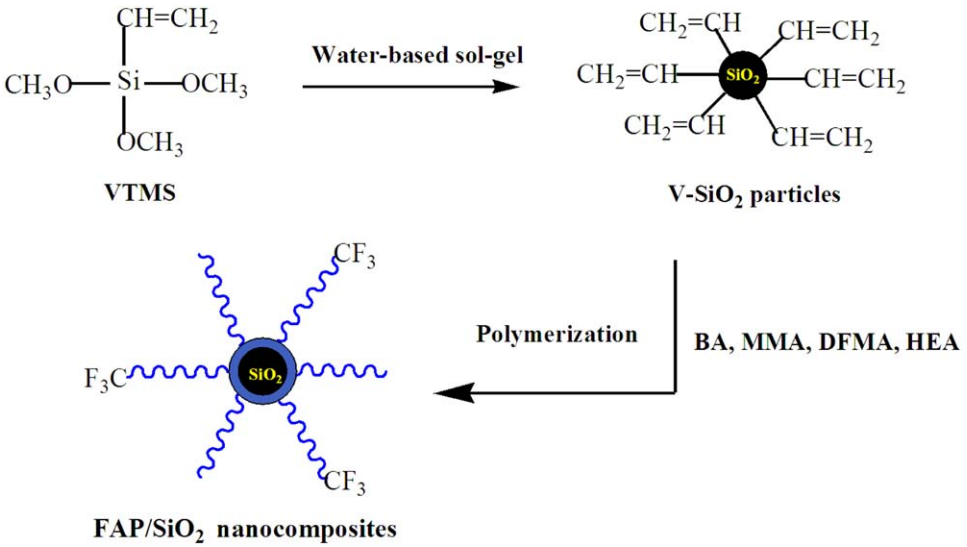

Figure 1. Preparation of FAP/SiO_2 nanocomposites. [Color figure can be viewed in the online issue, which is available at wileyonlinelibrary.com.]

5 min in the presence of weak alkali (pH: 8–9), respectively, and then squeezed using an automatic padder (Rapid Labortex, Taipei, Taiwan) with a nip pressure of 2 kg/cm^2. This process was repeated two times. The fabrics were then dried at 80°C for 5 min and cured at 160°C for 3 min in an oven.

Characterization

Fourier transform infrared spectrometry (FTIR) spectra were recorded on a 640 FTIR (Varian, America) using KBr crystal in the infrared region 4000–400 cm^{-1}. The particle size was measured by Zetasizer Nano ZS Particle Size Analyzer (Zetasizer Nano ZS, Malvern, Britain). The thermal stability was characterized by thermal gravimetric (TG) analysis, which was conducted under nitrogen atmosphere at a heating rate of 10°C/min with a TG209F1 thermogravimetric analyzer (Iris, Germany). The PET fabrics were characterized by scanning electron microscope (SEM, JSM-5600LV), scanning probe microscopy (SPM, NanoScope IV, room temperature), and X-ray photoelectron spectroscopy (XPS, XSAM800, Kratos, UK). The static wettability of the treated PET fabrics was characterized by the WCA measurement on an OCA40 contact angle system (Dataphysics, Germany) using a 5 μL water droplet at ambient temperature. The dynamic wettability of the treated PET fabrics was investigated by the water shedding angle (WSA) measurement and spray testing (AATCC Test Method 22–2005). The WSA was measured using a 15 μL water droplet according to the new technique introduced by Zimmermann et al.[40] As for the AATCC Test Method, the water repellency rating (WRR) is used to examine the extent of the wetting. The higher rating indicates higher hydrophobicity.

RESULTS AND DISCUSSION

Preparation of V—SiO_2 Nanoparticles

Compared with the traditional sol-gel reaction for the preparation of modified silica particles usually involving the preparation of silica followed by modification, in this study the vinyl nanosilica (V—SiO_2) hydrosols were prepared by one-step sol-gel process using VTMS as the precursor and ammonium hydroxide as the catalyst in the presence of composite surfactant AEO-9/SDBS, and water was used as solvent instead of ethanol. VTMS is insoluble in water. After VTMS and AEO-9/SDBS were mixed in water under vigorous stirring, the composite surfactant was adsorbed on the VTMS-water interface, reducing the interfacial tension and leading to the uniform dispersion of VTMS in micelle systems. When $NH_3 \cdot H_2O$ as the catalyst was added to the mixture solution, the water-based sol-gel reaction took place in the micelles microreactors, including the hydrolysis and condensation as indicated in Figure 2.

The base-catalyzed hydrolysis occurs based on a nucleophilic substitution mechanism.[41] OH^- attacks the silicon atom, resulting in the break of the Si—OCH_3 bond, forming Si—OH. Three methoxy groups of VTMS molecule are easily changed to hydroxyl groups, librating methanol as a byproduct (Figure 2). It was reported that methanol could help the VTMS precursor to be fully dissolved into water,[42] thus promoting the hydrolysis reaction. The deprotonated silanol under the alkaline condition is bound to attack protonated silanol or a methoxysilane group to form Si—O—Si bonds by condensation reaction, producing water or methanol, respectively, as shown in Figure 2. As a result, the monodisperse vinyl-functionalized SiO_2 particles were obtained.

Size Distribution Analysis

The size distribution by intensity of the V—SiO_2 hydrosol, FAP/SiO_2 nanocomposites and FAP were measured by Zetasizer Nano ZS Particle Size Analyzer. As can be seen in Figure 3, the average diameter of the prepared V—SiO_2 particles was 65.5 nm and the corresponding polydispersity index (PDI) was 0.098, indicating that the V—SiO_2 hydrosol was quite monodisperse and had relatively narrow size distribution. The average particle size of FAP was 75.39 nm with PDI of 0.176. As for the FAP/SiO_2 nanocomposites, the PDI was 0.223, and the particle size ranged from 100 nm to 150 nm with relatively narrow size distribution. The average particle size of the FAP/SiO_2 was 120.3

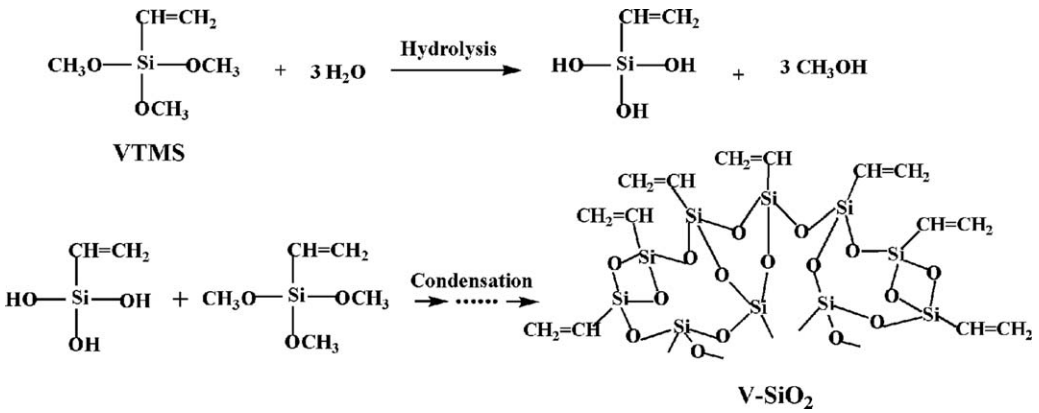

Figure 2. The water-based hydrolysis and condensation reaction of VTMS.

nm, larger than V—SiO_2 and FAP, which may indicate that the FAP/SiO_2 nanocomposites prepared by emulsion polymerization are based on the V—SiO_2 nanoparticles.

Fourier Transform Infrared Spectrometry

Figure 4 showed the FTIR spectra of V—SiO_2, FAP, and FAP/SiO_2. The characteristic absorption band of C=C at 1630 cm^{-1} can be observed in Figure 4(a). The bands of 1133–1048, 769, and 556 cm^{-1} were, respectively, attributed to Si—O—Si asymmetrical stretch vibrations, symmetrical stretch vibrations and bend vibrations. The peak at 1409 cm^{-1} belonged to Si—CH=CH_2 absorption peak. The presence of the band at 3441 cm^{-1} was ascribed to —OH vibration peak. These bands may indicate the successful preparation of vinyl functionalized nanosilica.

In FTIR spectra of FAP and FAP/SiO_2 [Figure 4(b,c)], the band of C=C at 1630 cm^{-1} was not detected, indicating that all the monomers had participated in polymerization reaction. There were some similar absorption bands in FTIR spectra of FAP and FAP/SiO_2, including the C=O characteristic absorption peak at 1737 cm^{-1}, the —OH stretch vibration peak attributed to the monomer HEA at 3444 cm^{-1}, the —CH_3 and —CH_2 stretch vibration peak at 2962 cm^{-1}, and the absorption band of C—F at 687 cm^{-1}.

Compared with the FTIR spectra of FAP, the absorption bands at 1246–1052 cm^{-1} in FTIR spectra of FAP/SiO_2 was stronger as a result of overlapping peaks of C—F groups, C—O—C stretch vibration and Si—O—Si absorption. The new strong absorptions appeared at 763 and 556 cm^{-1} in Figure 4(c), which belonged to Si—O—Si groups. It was shown that there were characteristic absorption bands of silica and fluorinated acrylate polymer in the FTIR spectra of FAP/SiO_2, indicating that V—SiO_2 had been polymerized with monomers like BA, MMA, HEA, and DFMA, and FAP containing short fluoroalkyl chains had been chemically bonded with nano SiO_2.

Thermal Gravimetric

The thermal stabilities of V—SiO_2, FAP/SiO_2, and FAP were investigated by TG. From Figure 5, thermal weight loss of V—SiO_2 below 300°C represented desorption of free water or small molecules and condensation of residual Si—OH groups on V—SiO_2 surface. The remaining weight percentage of V—SiO_2 was 63.02% after being heated to 800°C, probably due to the thermal decomposition of the C=C double bond. For

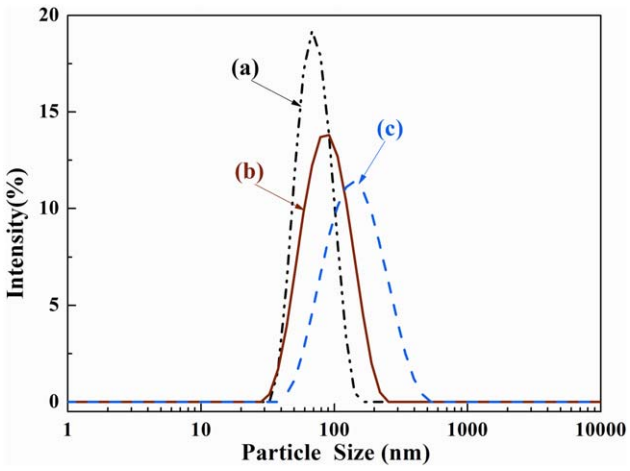

Figure 3. The size distribution by intensity: (a) V—SiO_2, (b) FAP, and (c) FAP/SiO_2. [Color figure can be viewed in the online issue, which is available at wileyonlinelibrary.com.]

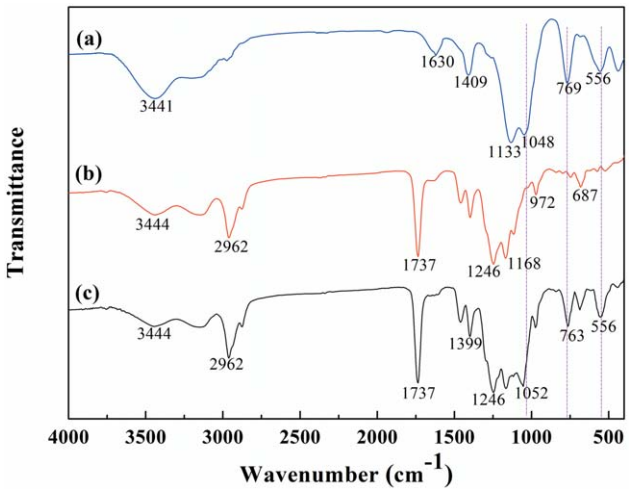

Figure 4. FTIR spectra of (a) V—SiO_2, (b) FAP, and (c) FAP/SiO_2. [Color figure can be viewed in the online issue, which is available at wileyonlinelibrary.com.]

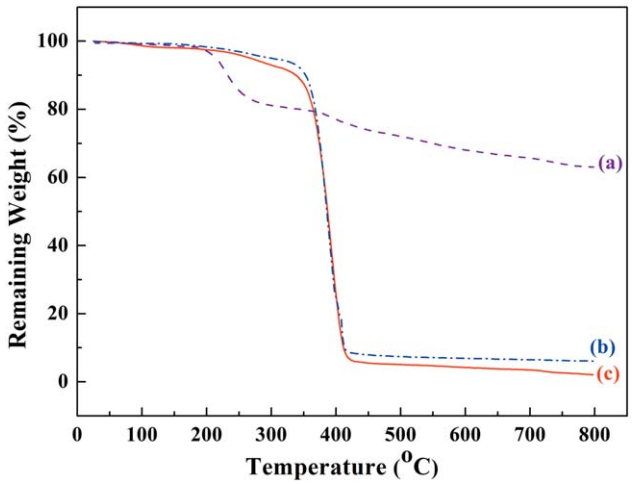

Figure 5. TG curves of (a) V—SiO_2, (b) FAP/SiO_2, and (c) FAP. [Color figure can be viewed in the online issue, which is available at wileyonlinelibrary.com.]

the TG curves of FAP/SiO_2 and FAP, when the weight loss was 10%, the decomposition temperatures of FAP/SiO_2 and FAP were 337 and 304°C, respectively. The remaining weight of FAP/SiO_2 was 6.09% after being heated to 800°C, which was much higher than that of FAP, while the remaining weight of FAP was 2.04%.

Therefore, the incorporation of SiO_2 nanoparticles greatly improved the thermal stability of FAP/SiO_2 nanocomposites. The reasons may be as follows. However, SiO_2 nanoparticles inherently have high strength, high toughness, and excellent thermal stability. However, SiO_2 nanoparticles with unique small size effect and macroscopical quantum tunnel effect were introduced into the FAP polymer chains, forming the FAP/SiO_2 nanocomposites. A defining feature of FAP/SiO_2 nanocomposites is that the small size of the SiO_2 nanoparticles leads to a dramatic increase in interfacial area as compared with traditional composites, to some extent, resulting in an increase in the crosslinking between FAP polymer matrix and the inorganic nanoparticles.[43] The SiO_2 nanoparticles have the "bridge" crosslinking in the FAP matrix. This chemical crosslinking could inhibit the thermal motion of polymer molecules. Thereby the introduction of nanometer-sized SiO_2 inorganic particles into the FAP polymer matrix could enhance thermal stability by acting as a superior insulator and mass transport barrier to the volatile products generated during decomposition.[43,44]

Coating of FAP/SiO_2 Nanocomposites onto PET Fiber

The FAP/SiO_2 nanocomposites were coated onto the PET fabric samples, including three different stages. As shown in Figure 6, the first stage was the dip-pad process. The PET fabric was dipped and padded by FAP/SiO_2 composite emulsion, and FAP/SiO_2 nanocomposites were distributed on the surface of PET fiber. The second stage was drying. When the PET fabric was dried at 80°C for 5 min, with the evaporation of water, the FAP/SiO_2 nanocomposites on PET fiber surface gradually moved closer and were closely arranged. The third stage was curing. The PET fabric was cured at 160°C for 3 min, leading to the coalescence of FAP/SiO_2 nanocomposites and interdiffusion and winding of FAP polymer molecular chains. As a result, molecular chains containing fluorine groups with lower surface energy migrated to the outmost surface and then were

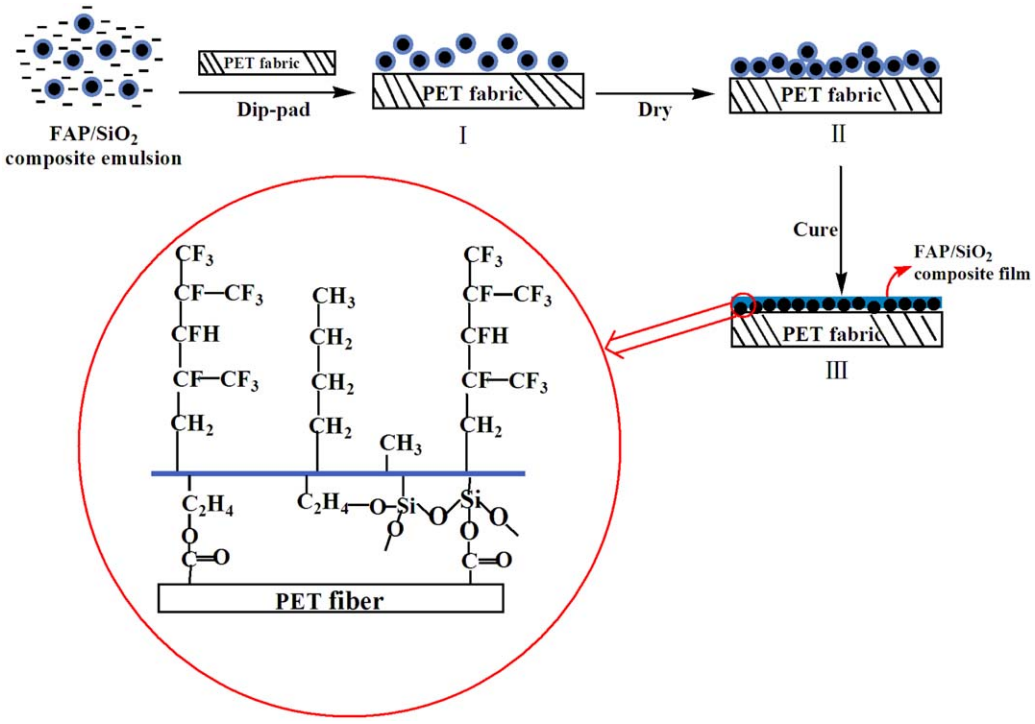

Figure 6. Schematic illustration of coating of FAP/SiO_2 nanocomposites onto PET fabric. [Color figure can be viewed in the online issue, which is available at wileyonlinelibrary.com.]

Table I. The Water Repellence of PET Fabrics Treated by FAP and FAP/SiO_2

Samples	WCA (°)	WSA (°)	WRR
PET fabric treated by FAP	132.3 ± 0.9	30 ± 0.7	75
PET fabric treated by FAP/SiO_2	151.5 ± 1.1	12 ± 0.6	95

perpendicular to the PET fabric surface, resulting in the dense arrangement and alignment of fluorine layer. The SiO_2 nanoparticles kept spherical, rendering the PET fabric surface rough. Therefore, FAP/SiO_2 film with low surface energy and roughness was formed on the PET fabric surface.

For coating of FAP/SiO_2 nanocomposites onto PET Fiber, hydroxyl groups in acrylate monomer HEA could react with the Si—OH groups on V—SiO_2 particles, forming a crosslinked network structure, thus improving adhesion ability of FAP/SiO_2 film on PET Fiber. Furthermore, PET fibers could partially hydrolyze under alkaline condition to generate surface carboxylic groups, which could subsequently cocondense with the Si—OH groups on V—SiO_2 particles and hydroxyl groups in HEA, leading to the formation of interfacial ester bonds.[45] As a result, FAP/SiO_2 nanocomposites could be chemically linked with the PET fabric, as demonstrated in Figure 6.

Surface Wetting Property

When the water drop was dripped on the untreated PET fabric, it would vanish rapidly. The static wettability of the PET sample was evaluated by WCA, while the dynamic wettability was investigated by the WSA measurement and spray testing (AATCC Test Method 22-2005). The water repellences of PET fabrics coated by the same concentration of FAP/SiO_2 nanocomposites and FAP were shown in Table I. PET fabric treated by FAP with low surface energy had a WCA of 132.3 ± 0.9°, a WSA of 30 ± 0.7° and WRR of 75, indicating that it is difficult to achieve superhydrophobicity only by reducing the surface tension.

In comparison, the PET fabric sample coated by FAP/SiO_2 nanocomposites displayed excellent superhydrophobicity with a WCA of 151.5 ± 1.1° (Figure 7), a WSA of 12 ± 0.6° (Figure 8), and WRR of 95, due to the combination of low surface energy and surface roughness. Figure 8 showed that a water droplet (15 μL) rolled off on the PET fabric treated by FAP/SiO_2 with a tilt angle of 12° at different time points. The water drop dripped on the fabric immediately rolled off the treated PET fabric, showing excellent dynamic hydrophobic properties.

Therefore, it can be concluded that superhydrophobic PET surfaces could be fabricated by coating the prepared FAP/SiO_2 nanocomposites. The introduction of nanosilica could improve the hydrophobicity of FAP/SiO_2 nanocomposites films. There may be several reasons. First, due to the nanoscale silica introduction, the physical and chemical crosslinkage of FAP increases as FAP polymer chains with low surface energy twist on the surface of nanosilica. Second, the Si—O—Si bonds also inherently have the hydrophobic effects. Third, the incorporation of spherical SiO_2 nanoparticles with unique small size effect and macroscopical quantum tunnel effect acts as protuberance on the surface of FAP/SiO_2 composite films, resulting in the increase of the surface roughness and the decrease of surface-free energy.[34]

When the PET fabric was coated by the FAP/SiO_2 nanocomposites, the presence of these SiO_2 nanoparticles made microscale PET fiber surface become uneven, thus generating a dual-size rough surface structure on the PET fabric. These rough structures based on the SiO_2 nanoparticles were covered with hydrophobic fluorinated polymer layer. The nanoscale silica stacking generates an essential roughness for the large air pockets.[46] When a water droplet sits on the rough surface of the treated PET fabric, a larger amount of air film can be trapped in the nanostructural texture as the nanoparticles with large interfacial area can adsorb gas molecules and make gas molecules stable, producing a water-air-solid interface. Thus, the water drop only contacts the top of the asperities due to the existence of an air film, which protects the PET substrate against water penetration.

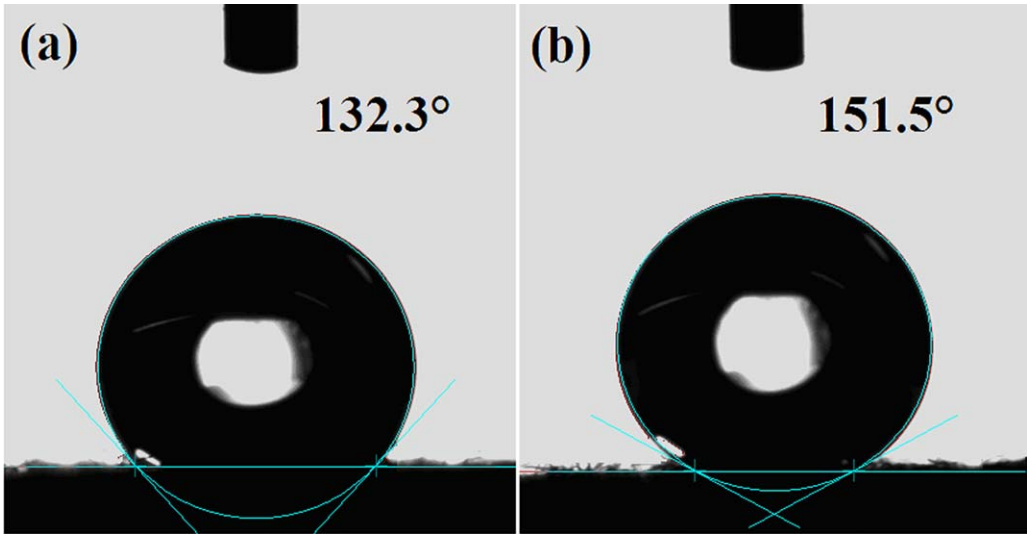

Figure 7. Images of a water droplet (5 μL) on: (a) PET fabric treated by FAP and (b) PET fabric treated by FAP/SiO_2. [Color figure can be viewed in the online issue, which is available at wileyonlinelibrary.com.]

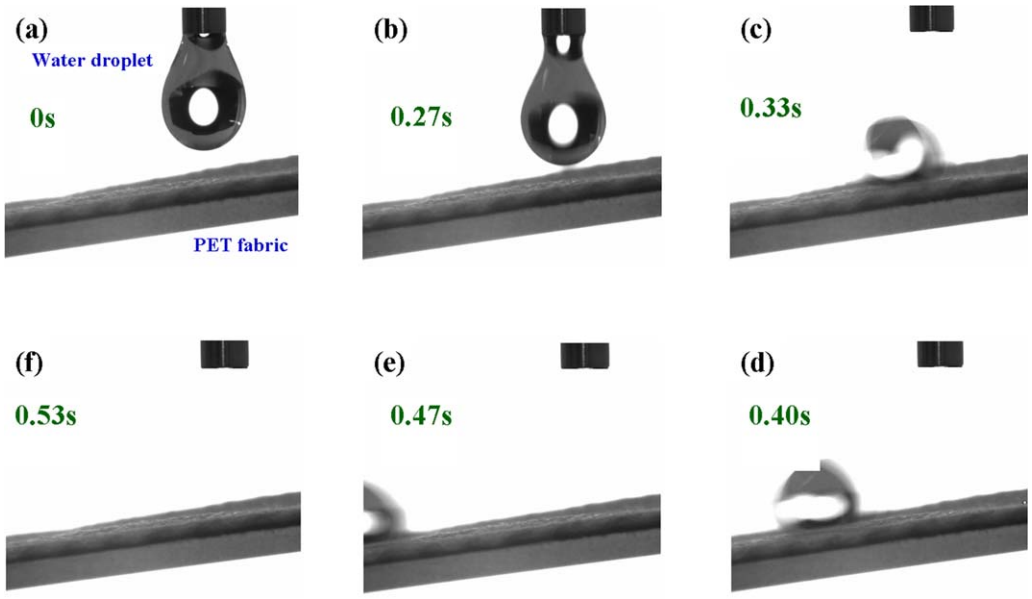

Figure 8. A water droplet (15 μL) rolled off on the PET fabric treated by FAP/SiO_2. [Color figure can be viewed in the online issue, which is available at wileyonlinelibrary.com.]

The water repellency of PET fabric treated by FAP/SiO_2 can be further explained by the Cassie-Baxter equation,[47] as described by the following equation.

$$\cos\theta_{CB} = f_{ls}\cos\theta_s + f_{lv}\cos\theta_v \quad (1)$$

where θ_{CB} is the apparent WCA on a rough surface, f_{ls} is the liquid/solid contact area divided by the projected area, and f_{lv} is the liquid/vapor contact area divided by the projected area ($f_{ls}+f_{lv}=1$). θ_s and θ_v ($\theta_v = 180°$) are the WCA on the smooth solid surface and vapor surface, respectively. The FAP/SiO_2 composite latex film on the smooth glass surface was measured to have a WCA of about 115.8° in our study. Here, it was approximately assumed that θ_s was 115.8°. As mentioned above, the superhydrophobic rough surface of the PET fabric treated by FAP/SiO_2 nanocomposites had a WCA of about 151.5° in our study. That is to say, θ_{CB} was 151.5°. According to the Cassie-Baxter equation, it was calculated that the liquid/vapor contact area divided by the projected area f_{lv} was 79%. Therefore, when a water droplet sits on the surface of PET fabric treated by FAP/SiO_2 nanocomposites, the large fraction of air is trapped underneath the water droplet, effectively repelling the water penetration. Hereby, the cooperation of surface roughness due to the SiO_2 nanoparticles and low surface energy because of the FAP containing short fluoroalkyl chains resulted in the achievement of superhydrophobic PET fabric.

Surface Morphology

SEM and SPM were used to observe the surface morphology of the PET fabrics treated by FAP and FAP/SiO_2. The original PET fabric has extremely smooth surface. As can be seen from Figure 9(a), PET fiber treated by FAP was relatively smooth caused by coating of a layer of FAP on the surface of the PET fiber. However, PET fibers treated by FAP/SiO_2 became much rougher with a particulate surface, due to the introduction of nanoparticles.

As shown in Figure 10(a), the SPM image of PET fabric treated by FAP also indicated some ceraceous matters appeared on the

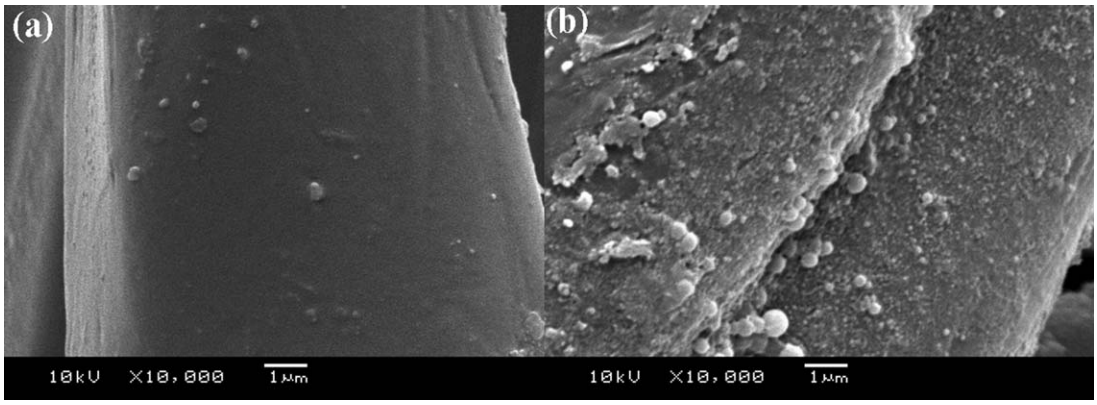

Figure 9. SEM images of PET fabrics treated by (a) FAP and (b) FAP/SiO_2.

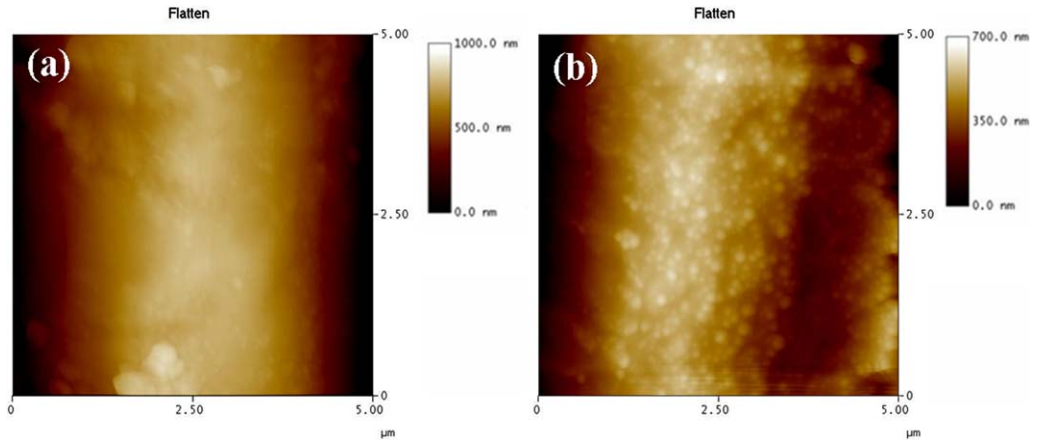

Figure 10. SPM images of PET fabrics treated by (a) FAP and (b) FAP/SiO_2. [Color figure can be viewed in the online issue, which is available at wileyonlinelibrary.com.]

relatively smooth PET surface. By contrast, appropriate unevenness and close-packing nanoparticles occurred on the surface of the PET fiber treated by FAP/SiO_2 in Figure 10(b). It was indicated that surface rough structure was realized on the PET fabric coated by FAP/SiO_2.

Surface Chemical Composition

The surface chemical composition of the treated PET fabric was characterized by XPS analysis. For the PET fabric treated by FAP, as shown in Figure 11(b), F1s, O1s, and C1s peaks were detected at around 689.1, 532.3, and 285.2 eV, respectively. In contrast, in the XPS spectra of the PET fabric treated by FAP/SiO_2 [Figure 11(a)], the additional characteristic peaks of Si2s and Si2p emerged at 156.2 and 102.6 eV. In addition, there was a large increase of the O1s peak intensity. The result may be explained that the inorganic component SiO_2 nanoparticles of FAP/SiO_2 nanocomposites lead to the introduction of Si and O element and the higher O1s peak intensity in the XPS spectra of the PET fabric treated by FAP/SiO_2. This measurement further confirmed the successful incorporation of the SiO_2 nanoparticles into the FAP/SiO_2 nanocomposites.

As shown in Figure 12, the C1s XPS spectra of PET fabric treated by FAP/SiO_2 at high-resolution had five subpeaks, which stand for five kinds of carbon bonds. The bands at 293.6, 289.3, 287.5, 286.0, and 284.8eV were attributed to —CF_3, —CF, C═O, C—O, and C—C, respectively, indicating a strong surface enrichment of fluorine, due to the migration of fluorinated side chains to the surface so as to minimize interfacial free energy.[48] In other words, it was revealed that the fluoroacrylic monomer DFMA had involved the polymerization to prepare FAP/SiO_2 nanocomposites.

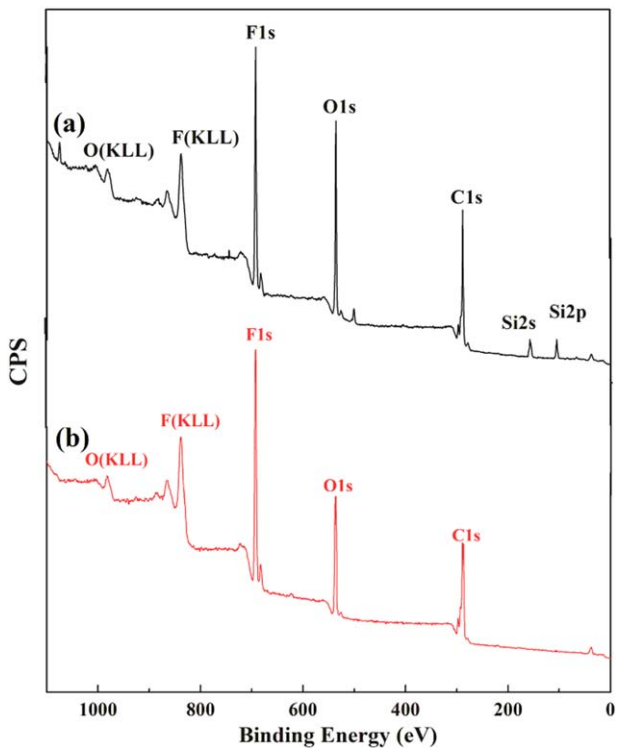

Figure 11. XPS spectra of PET fabrics treated by (a) FAP/SiO_2 and (b) FAP. [Color figure can be viewed in the online issue, which is available at wileyonlinelibrary.com.]

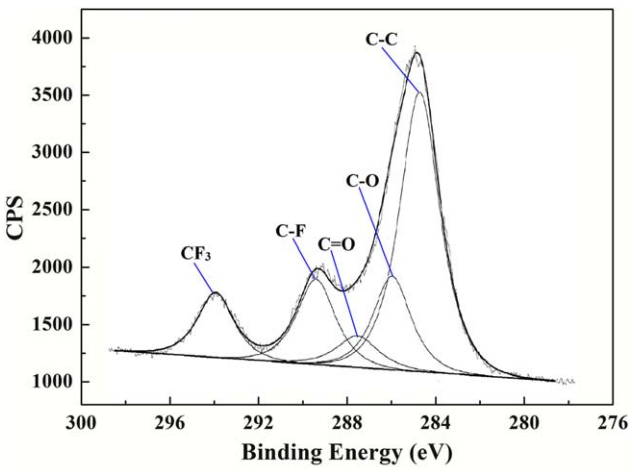

Figure 12. The C1s XPS spectra of PET fabric treated by FAP/SiO_2. [Color figure can be viewed in the online issue, which is available at wileyonlinelibrary.com.]

CONCLUSIONS

This study presented a novel method to prepare superhydrophobic PET fabrics by coating FAP/SiO_2 nanocomposites. The FAP/SiO_2 nanocomposites were synthesized via emulsion polymerization based on V—SiO_2 hydrosol, which was prepared by one-step water-based sol-gel method using VTMS as the precursor. The V—SiO_2 nanoparticles had been successfully introduced into the FAP/SiO_2 nanocomposites, improving the thermal stability and surface roughness of FAP/SiO_2 nanocomposites. The obtained V—SiO_2 hydrosol and FAP/SiO_2 nanocomposites had relatively narrow size distribution. The FAP/SiO_2 nanocomposites were applied to the PET fabrics by dip-pad-cure process. The coated PET fabrics exhibited excellent superhydrophobicity with a WCA of 151.5° for a 5 μL water droplet and a WSA of 12° for a 15 μL, due to the synergistic effect of the dual-size rough surface structure provided by the SiO_2 nanoparticles on microscale PET fiber and the low surface energy caused by fluorinated polymers FAP, as confirmed by SEM, SPM, and XPS. This approach is facile and reveals a true potential for hybrid materials to generate superhydrophobic surfaces.

ACKNOWLEDGEMENT

This research was supported by Innovation Program of Shanghai Municipal Education Commission (12ZZ180). This research was also supported by Shanghai Cultivation Funding Program for Young College Teachers (ZZGJD13038).

REFERENCES

1. Raza, M. A.; Kooij, E. S.; van Silfhout, A.; Poelsema, B. *Langmuir* **2010**, *26*, 12962.
2. Chang, K. C.; Chen, H.; Huang, C. K.; Huang, S. I. *J. Appl. Polym. Sci.* **2007**, *104*, 1646.
3. Richard, E.; Lakshmi, R. V.; Aruna, S. T.; Basu, B. J. *Appl. Surf. Sci.* **2013**, *277*, 302.
4. Hsieh, C. T.; Wu, F. L.; Chen, W. Y. *Mater. Chem. Phys.* **2010**, *121*, 14.
5. Zou, H.; Lin, S.; Tu, Y.; Liu, G.; Hu, J.; Li, F.; Miao, L.; Zhang, G.; Luo, H.; Liu, F., Hou C, Hu M. *J. Mater. Chem. A* **2013**, *1*, 11246.
6. Gao, Y.; Huang, Y. G.; Feng, S. J.; Gu, G. T.; Qing, F. L. *J. Mater. Sci.* **2010**, *45*, 460.
7. Bae, G. Y.; Min, B. G.; Jeong, Y. G.; Lee, S. C.; Jang, J. H.; Koo, G. H. *J. Colloid Interface Sci.* **2009**, *337*, 170.
8. Hoefnagels, H. F.; Wu, D.; de With, G.; Ming, W. *Langmuir* **2007**, *23*, 13158.
9. Hsieh, C. T.; Wu, F. L.; Yang, S. Y. *Surf. Coat. Technol.* **2008**, *202*, 6103.
10. Lakshmi, R. V.; Bharathidasan, T.; Bera, P.; Basu, B. J. *Surf. Coat. Technol.* **2012**, *206*, 3888.
11. An, Q. F.; Xu, W.; Hao, L. F.; Fu, Y. S.; Huang, L. X. *J. Appl. Polym. Sci.* **2013**, *128*, 3050.
12. Xue, C. H.; Jia, S. T.; Chen, H. Z.; Wang, M. *Sci. Technol. Adv. Mater.* **2008**, *9*, 1.
13. Zhang, X.; Guo, Y.; Zhang, Z.; Zhang, P. *Appl. Surf. Sci.* **2013**, *284*, 319.
14. Zhang, Y.; Li, S.; Huang, F.; Wang, F.; Duan, W.; Li, J.; Shen, Y.; Xie, A. *Russ. J. Phys. Chem. A* **2012**, *86*, 413.
15. Ashraf, M.; Campagne, C.; Perwuelz, A.; Champagne, P.; Leriche, A.; Courtois, C. *J. Colloid Interface Sci.* **2013**, *394*, 545.
16. Preda, N.; Enculescu, M.; Zgura, I.; Socol, M.; Matei, E.; Vasilache, V.; Enculescu, I. *Mater. Chem. Phys.* **2013**, *138*, 253.
17. Xu, B.; Cai, Z. S.; Wang, W. M.;Ge, F. Y. *Surf. Coat. Technol.* **2010**, *204*, 1556.
18. Wang, T.; Hu, X. G.; Dong, S. J. *Chem. Commun.* **2007**, 1849.
19. Shateri-Khalilabad, M.; Yazdanshenas, M. E. *J. Text. Inst.* **2013**, *104*, 861.
20. Richard, E.; Aruna, S. T.; Basu, B. J. *Appl. Surf. Sci.* **2012**, *258*, 10199.
21. Li, G.; Wang, H.; Zheng, H.; Bai, R. *Langmuir* **2010**, *26*, 7529.
22. Wang, K.; Hu, N. X.; Xu, G.; Qi, Y. *Carbon* **2011**, *49*, 1769.
23. Jiang, C.; Zhang, Y.; Wang, Q.; Wang, T. *J. Appl. Polym. Sci.* **2013**, *129*, 2959.
24. Sun, X. L.; Fan, Z. P.; Zhang, L. D.; Wang, L.; Wei, Z. J.; Wang, X. Q.; Liu, W. L. *Appl. Surf. Sci.* **2011**, *257*, 2308.
25. Zhang, M.; Wang, C.; Wang, S.; Li, J. *Carbohydr. Polym.* **2013**, *97*, 59.
26. Misra, R.; Cook, R.D.; Morgan, S.E. *J. Appl. Polym. Sci.***2010**, *115*, 2322.
27. Yang H.; Hu X. J.; Chen R.; Liu S. T.; Pi P.H.; Yang Z. R. *Appl. Surf. Sci.* **2013**, *280*, 113.
28. Basu, B. B. J.; Paranthaman, A. K. *Appl. Surf. Sci.* **2009**, *255*, 4479.
29. Hsieh, C. T.; Chang, B. S.; Lin, J. Y. *Appl. Surf. Sci.* **2011**, *257*, 7997.
30. Yu, H. J.; Luo, Z. H. *J. Polym. Sci. Part A Polym. Chem.* **2010**, *48*, 5570.
31. Chen, Z. M.; Pan, S. J.; Yin, H. J.; Zhang, L. L.; Ou, E. C.; Xiong, Y. Q.; Xu, W. J. *Express Polym. Lett.* **2011**, *5*, 38.
32. Qu, A. L.; Wen, X. F.; Pi, P. H.; Cheng, J.; Yang, Z. R. *J. Mater. Sci. Technol.* **2008**, *24*, 693.
33. Cui, X.; Zhong, S.; Yan, J.; Wang, C.; Zhang, H.; Wang, H. *Colloids Surf. A* **2010**, *360*, 41.
34. Yao, L.; Yang, T. T.; Cheng, S. Y. *J. Appl. Polym. Sci.* **2010**, *115*, 3500–3507.
35. Liu, X. Y.; Zhao, H. P.; Li, L.; Yan, J.; Zha, L. S. *J. Macromol. Sci. Chem.* **2006**, *43*, 1757.
36. Wen, X. F.; Li, M. Z.; Pi, P. H.; Chen, J.; Yang, Z. R. *Colloid Surf. A* **2008**, *327*, 103.
37. Nassar, E. J.; Nassor, E. C. D.; Avila, L. R.; Pereira, P. F. S.; Cestari, A.; Luz, L. M.; Ciuffi, K. J.; Calefi, P. S. *J. Sol-Gel Sci. Technol.* **2007**, *43*, 21.
38. Riccio, D. A.; Nugent, J. L.; Schoenfisch, M. H. *Chem. Mater.* **2011**, *23*, 1727.

39. Chen, S.; Hayakawa, S.; Shirosaki, Y.; Fujii, E.; Kawabata, K.; Tsuru, K.; Osaka, A. *J. Am. Ceram. Soc.* **2009**, *92*, 2074.
40. Zimmermann, J.; Seeger, S.; Reifler, F. A. *Text. Res. J.* **2009**, *79*, 1565.
41. Arriagada, F. J.; Osseo-Asare, K. *J. Colloid Interface Sci.* **1999**, *211*, 210.
42. Sankaraiah, S.; Lee, J. M.; Kim, J. H.; Choi, S. W. *Macromolecules* **2008**, *41*, 6195.
43. Zou, H.; Wu, S. S.; Shen, J. *Chem. Rev.* **2008**, *108*, 3893.
44. Ray, S. S.; Okamoto M. *Prog. Polym. Sci.* **2003**, *28*, 1539.
45. Hernandez-Padron, G.; Rojas, F.; Castano, V. M. *Nanotechnology* **2004**, *15*, 98.
46. Hsieh, C. T.; Wu, F. L.; Chen, W. Y. *Surf. Coat. Technol.* **2009**, *203*, 3377.
47. Cassie, A. B. D.; Baxter, S. *Trans. Faraday Soc.* **1944**, *40*, 546.
48. Yang, H.; Pi, P. H.; Wen, X. F.; Zheng, D. F.; Cheng, J. A.; Yang, Z. R. *Prog. Chem.* **2010**, *22*, 1133.